International Journal of Aeronautical and Space Sciences (2018) 19:584–594
https://doi.org/10.1007/s42405-018-0054-y

IJASS International Journal of Aeronautical and Space Sciences

ORIGINAL PAPER

Dynamic Response of Low-Aspect-Ratio Cantilever NACA0012 Airfoil at Low-To-Moderate Reynolds Numbers

S. Martínez-Aranda[1] · A. García-González[2] · L. Parras[2] · J. F. Velazquez-Navarro[2] · C. del Pino[2]

Received: 11 February 2017 / Revised: 23 February 2018 / Accepted: 28 May 2018 / Published online: 3 August 2018

Abstract
The influence of the angle of attack (AoA) and the chord based Reynolds number (Re_c) on the lift and drag coefficients has been analyzed experimentally in a low-aspect-ratio NACA0012 airfoil, AR = 2. Results are shown for chord based Reynolds numbers in the range $3.33 \times 10^4 \leq Re_c \leq 1.33 \times 10^5$ and AoA between 0º and +35º, the stall angle being close to 12º. The aerodynamic characteristics show an increase and decrease of lift and drag force fluctuations for AoA greater than the stall angle. The explanation of how these aerodynamic variations appear has been reported numerically and it is based on two-dimensional effects which are mainly the unstable laminar separation bubble (LSB) and the subsequent downstream propagation of leading edge vortex (LEV) as AoA increases. In addition, the dynamic response of the wing has been studied using frequency analysis. We compute the power spectral density (PSD) from the temporal evolution of the net force exerted over the wing, showing that the main response of the wing is the presence of two natural frequencies of the wing-base system. The mean PSD suddenly increases for $Re_c \approx 1 \times 10^5$, particularly at AoA exceeding the critical point that corresponds to the stall angle. Finally, and despite from the fact that our model is rigid, we find PSD peaks at very low and high frequencies in agreement with other authors' results which correspond to energetic modes in the wingtip vortex and the formation and emission of coherent turbulent structures behind the airfoil, respectively.

Keywords Finite wing · Low re aerodynamics · Wingtip vortex · Dynamic response

1 Introduction

The values of drag and lift coefficients of finite wing profiles vary mainly due to three mechanisms: presence of wingtip vortex [1–4]; laminar boundary layer separation leading to the formation of a laminar separation bubble (LSB) and the subsequent turbulent separated shear layer [5–7]; and, finally, the vortex shedding in the wake behind the wing [8–11]. Most of these numerical or experimental investigations have been performed analyzing only the flow behavior. Hence, the C and C_L experimental measurements involve a whole fluid–structure interaction scenario, giving us an overview of the iDnteraction between the wing and the flow that passes over it. The aim of the present analysis is to study the possible relationships among wingtip vortex, surface flow regimes, wake vortex and structural dynamic response of low-aspect-ratio cantilever NACA 0012 airfoil at low-to-moderate Reynolds numbers. Besides, the motivation of this work is based on potential applications such us the verification of CFD codes to simulate the wakes in turbulent regime, and the existence of similarities and differences between mechanical vibrations and noise source plus their associated tonal modes.

The study of the dynamic response of rigid wing models, the flow behavior in the suction surface and the wake have been extensively studied for a wide range of airfoils at low Reynolds numbers [12] characterized the flow regimes in the suction surface of a NACA 0012 airfoil for $3 \times 10^4 < Re_c < 1.3 \times 10^5$ and AR = 5. Huang and Lin [8] reported that the evolution of vortex shedding behind the airfoil at small AoA is connected to the development of shear-layer instabilities. Coherent turbulent structures generated in the separated shear-layer region, interact in the turbulent wake creating a large-scale vortex with measured frequencies one order of magnitude lower than the fundamental frequency of the shear-layer disturbances. The vortex shedding frequency

✉ A. García-González
tolin@uma.es

[1] LIFTEC-CSIC, Universidad de Zaragoza, 50009 Saragossa, Spain

[2] Universidad de Málaga, E.T.S. Ingeniería Industrial, Campus de Teatinos, 29071 Málaga, Spain

behind a NACA 0012 airfoil was also measured by [9]. Four emission modes were identified: laminar, subcritical, transitional and supercritical [11] identified numerically frequency peaks before and after the stall angle for a NACA 0012 airfoil using direct numerical simulations (DNS) at $Re_c = 5 \times 10^4$. More recent [13] studied numerically the effect of airfoil thickness on the onset of dynamic stall. They found that the presence of the unstable LSB followed by flow reversal boundary is linked to the stall. In particular, they showed contours of span-averaged pressure and skin friction coefficients on the suction side through the constant-rate pitch-up motion which behave very different for a wide range of AoA after the stall angle. These numerical data require, however, further experimental validation specially because these simulations were carried out for fully turbulent flows.

There are experimental data for 2D NACA 0012 airfoils mounted on two supports and covering low Reynolds numbers between 5.3×10^3 and 5.1×10^4 [14, 15]. It has been also studied the pitching oscillation of NACA0012 airfoils [16–18], but these self-sustained oscillation analyses differ from the dynamic response presented in this paper. Actually, the boundary conditions are completely different, because these airfoils have both edges attached, so that wingtip vortex formation is neglected and this does not occur in the present study. There are recent studies concerning experimental modal analysis for low- aspect-ratio rectangular membrane wings [19, 20]. These modal analyses were performed by means of digital image correlation (DIC) technique so, in this case, deformation data were reported and no forces were measured. The ratio between wing deformations and the flow characteristics is also reported in the State of Art [19, 20] suggested a possible coupling between the membrane vibration with the onset of wake instabilities for all airfoils.

Other key aspect which has been studied in detail consists of the noise production as several types of NACA airfoils are immersed in turbulent flow streams [21–24]. Moreau analyzed the noise produced by finite airfoil at low-to-moderate reynolds numbers. Apart from the noise measurements, surface oil-film visualization images were also taken in order to determine flow mechanisms responsible of noise generation. In this manner, our research study is a complement to attain only an objective view of airfoil vibration. On the other hand, [22] studied the noise differences between straight and serrated trailing edges by means of particle imaging velocimetry (PIV) measurements of the NACA0012 airfoil wakes together with microphones. Besides, these authors found that small variations in AoA can lead to noise level increments due to laminar separation bubble. [24] carried out leading edge noise measurements on three different NACA airfoils immersed in a turbulent flow. Also, a noise increment with AoA was observed. As will be commented below, similar conclusions can be deducted from our experimental study. For this reason, our motivation is based on the belief that experimental information of wing profile vibrations would be relevant for problems of fluid–structure interaction (FSI), and numerical model validations which have been also used for airfoil noise estimation, e.g., [25] or [26] our style.

2 Aerodynamic Characteristics: Results and Discussion

Experimental tests set can be followed in previous papers (see [27, 28]). A schematic drawing is shown in Fig. 1. The turbulence level (Turbulence Intensity I_∞ (%)] is shown in Table 1. The chord based Reynolds number is defined as $Re_c = U_\infty \cdot c/\nu$ where U_∞, c and ν are the free-stream velocity, wing chord (100 mm) and temperature-dependent kinematic viscosity. The standard deviation of the tests will be presented and discussed below. The main difference with the last two references are explained as follows [27] explored in the same wind tunnel the performance of airflow and aerodynamic characteristics in two configurations: one flat plate and a cascade of flat plates. The lift coefficient for a plate in the cascade had a peak when the angle of attack was almost twice that above which the single plate became stalled for relatively low values of the aspect ratio and Reynolds number of $Re_c \sim O(10^5)$. This investigation was performed to better understand the efficiency in prototypes regarding potential devices designed to extract hydrokinetic energy from tidal and river currents. On the other hand, [28] aims to giving aerodynamics characteristics of the NACA 0012 wing model for any aspect ratio and Reynolds number. To that end, we show lift and drag coefficients as function of angle of attack before the stall angle, thus showing general correlations which are of great interest for designing or experimental verification. However, in this piece of research we analyze the dynamic response of the wing model NACA0012 for a wide range of angles of attack, including AoA lower and greater than the stall angle.

2.1 Coefficient Deviations and Errors

Figure 2a shows the data together with error bars that corresponds to standard deviations from the average values of the drag and lift coefficients as function of AoA for $\alpha = 0°$–$35°$ at Reynolds numbers $Re_c = 1.33 \times 10^5$, which represents the worst case dealing with measurement errors. Other cases analyzed in this work show a similar behavior. Actually, the deviation remains constant up to the stall angle ($\alpha \leq 12°$–$14°$) and these variations are close to ± 0.025 in both coefficients, C_L and C_D, as it can be also observed in Fig. 2b, c that absolute values of the standard deviations with AoA smaller than 12° are quite small for any value of the Reynolds numbers. However, we noticed that self-sustained oscillations in the cantilever together with great fluctuations appear in the

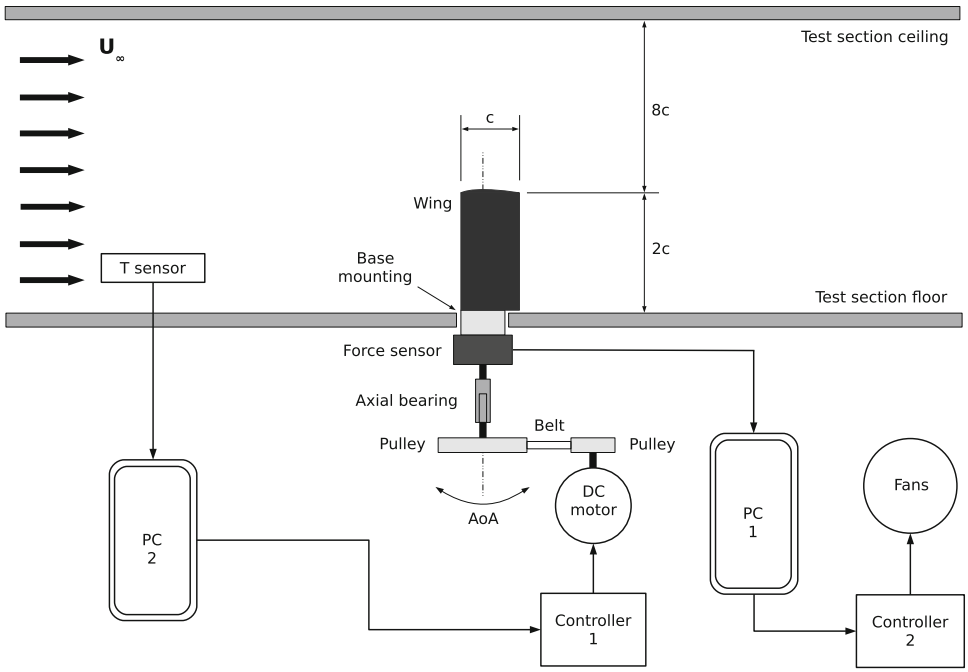

Fig. 1 Schematic of the experimental setup

Table 1 Free-stream wind velocities and their variations, chord based Reynolds numbers and levels of turbulence intensity

U_∞ (m/s)	δU_∞ (m/s)	Re_c	IU_∞ (%)
5	±0.06	3.33×10^4	1.2
10	±0.12	6.67×10^4	1.2
15	±0.16	1×10^5	1.1
20	±0.47	1.33×10^5	2.3

force signal for AoA equal to or slightly greater than stall, thus resulting in a sudden increment of the C_L and C_D deviations. The maximum values of coefficient deviations take place for AoA between 13° and 18°. These deviations in the coefficients gradually decrease at AoA roughly greater than 20° for any value of Re_c. Experimentally, one can observe in this last range of AoA an amplitude reduction in the wing model vibration, so that variations in the force amplitude diminish as well.

To sum up, the time evolution of the forces from the stall angle up to $\alpha^* = 16°–18°$ produces large amount of oscillations, so the standard deviation of the associated forces grows accordingly (see again Fig. 2a). The exact value of α^* depends on Re_c but it decreases with Re_c. However, there is a saturation of force measurement variations from angles of attack greater than 18°, and wing vibrations seem to be less visible in the experimental setup [13] studied the turbulent regime before and after stall angles for a 2D NACA0012 airfoil among other profiles. Numerical data showed that there is a large reverse flow in the (boundary layer) suction wall from angles of attack greater to 17.82º (see the Fig. 7e in this reference). This is also the consequence of the pulsating LSB and the downstream propagation of dynamic stall vortices located at the leading edge. More information is also given in this paper regarding the span-averaged pressure and skin friction coefficients on the suction side through the constant-rate pitch-up motion for any AoA. In these plots, there is a saturation of the coefficients in the same range of AoA considered in our experimental work. For this reason, there is a plausible explanation of the connection between the saturation in the force measurements and turbulent structure formed in the suction wall of the airfoil: unstable LSB and the subsequent LEV downstream propagation. For this reason, only these 2D effects but not those generated in the wingtip produce this reduction of wing vibrations [29]. Developed the method to compute the propagation of experimental measurement errors, so one can estimate the accuracy of the non-dimensional drag and lift coefficients. Considering their formulation to determine the aerodynamic coefficients, large percentage uncertainties appear for coefficients approaching zero. The accuracy of the force measurement is 0.01 N, the rotational device has a resolution of 0.1°, and the accuracy of the free-stream velocity using LDA is within 1% [30]. Table 2 shows the estimation of the average errors for C_D and C_L at each Reynolds number, thus confirming a good experimental procedure in the computation of these coefficients because the fluctuation measurements are done with acceptable precision. Only C_D and C_L average values will be presented in the following section.

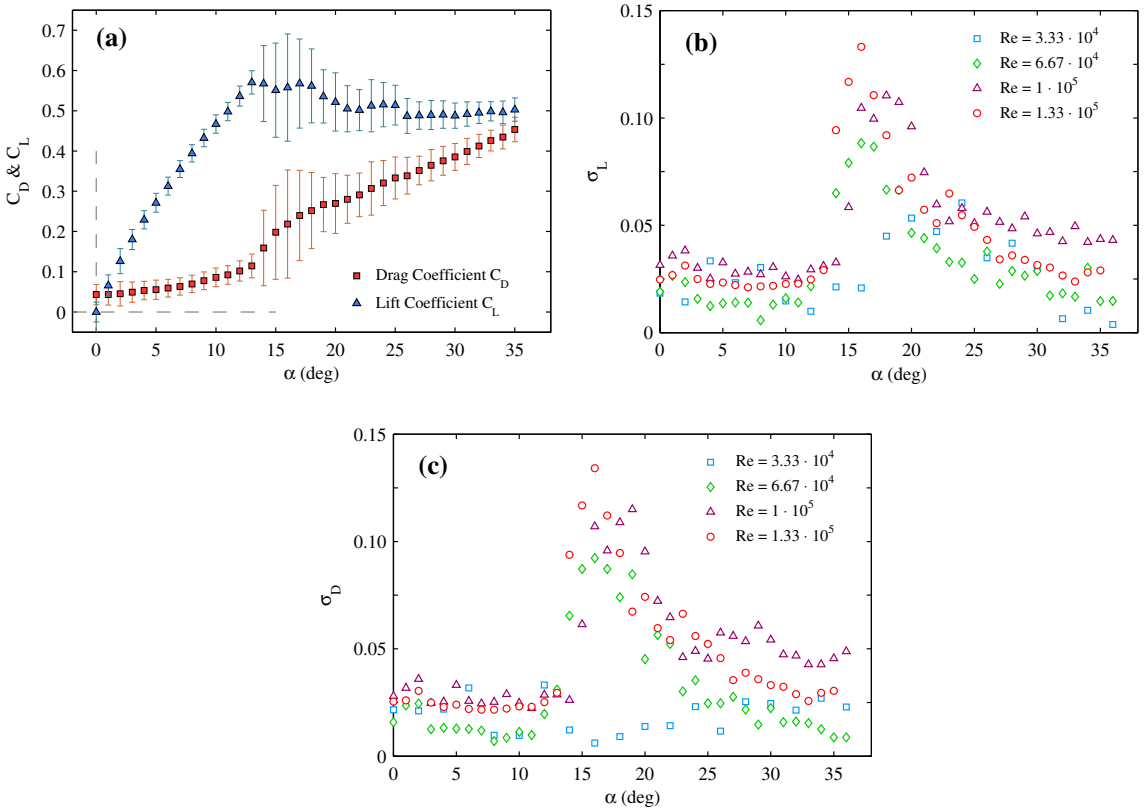

Fig. 2 Mean and standard deviation of C_D and C_L for $Re_c = 1.33 \times 10^5$ (**a**); standard deviations in the lift, σL (**b**) and drag, σD coefficients (**c**) for all AoA and Reynolds numbers

Table 2 Average errors for coefficients C_D and C_L

Re_c	% Error C_D	% Error C_L
3.33×10^4	$\pm$ 8.6	$\pm$6.2
6.67×10^4	$\pm$3.1	$\pm$ 2.0
1×10^5	$\pm$1.7	$\pm$1.3
1.33×10^5	$\pm$1.4	$\pm$1.2

2.2 Drag and Lift Curves

Drag coefficients are depicted in Fig. 3 as function of α. Our results show a slight deviation in comparison to those obtained by [31]. Besides, our values of C_{Dmin} are in agreement with those reported by [2] for a flat wing with the same aspect ratio and Reynolds numbers. Regarding the ratio between drag coefficient and AoA, C_D/α, we observe an increment of its value up to the stall angle, so that the wing loses its aerodynamic effectiveness. Different slopes are found at each Reynolds number, increasing the values of the slope with the AoA up to the stall angle.

The maximum lift coefficient C_{Lmax} ranges between 0.52 and 0.61 for any value of Re_c, and the stall angles α_{stall} appear between 12 and 14 degrees. These values show a slight deviation compared to those published by [31] with AR = 4 who reported a stall angle at 11°. As expected, our stall angles are slightly greater than Ngo's results due to the aspect ratio reduction (AR = 2 in our case). It is worth mentioning that the values of C_L are lower than those obtained by [2] for a flat plate with the same aspect ratio and Reynolds numbers.

3 Wing Dynamic Response: Results and Discussion

The temporal evolution of the force acting on the wing has been analyzed for any value of the AoA and four values of Re_c. We calculate the power spectral density (PSD) for each signal in the frequency domain by means of a FFT built-in Matlab® function. We subtract the mean force to the instantaneous one, thus obtaining the temporal evolution of the force and the most energetic frequencies. We observe that the sampling frequency of the force sensor is fs = 250 Hz, and the time recording of the tests is T = 200 s, hence the frequency resolution is $df = \pm 0.005$ Hz. We consider a low-pass filter in order to avoid aliasing effects in the digital signal. After applying this filter, the frequencies beyond the Nyquist ones are removed, being $F_{Nyquist}$ = fs/2.

We obtain the natural frequencies of the wing-base system with two sets of ten tests with no velocity inside the wind

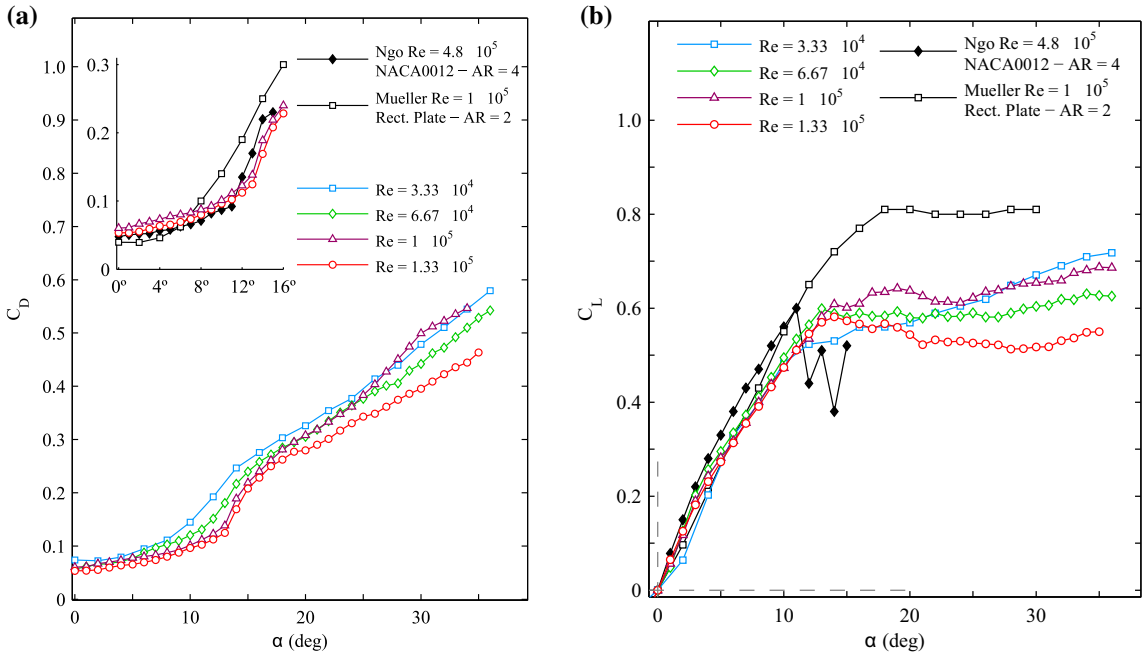

Fig. 3 C_D and C_L curves as function of α for all Reynolds numbers tested (**a**) C_D vs α for any value of the Reynolds numbers, as indicated. The inset represents a detail of C_D values for low AoA and high Reynolds numbers together with those reported by [27] and [26]. (**b**) C_L vs α for any value of the Reynolds numbers together with those reported by [27] and [26]

tunnel. The first testing consists of an instant impact at the free ending in the wing center following a direction perpendicular to the chord. Thus, the model vibrates freely and we record the net force. The temporal signal is analyzed by means of the FFT function. A main free vibration frequency is detected at $f_{1st} \approx 28.25$ Hz. The second testing consists of an instant impact at the cylindrical aluminum base which fixes the wing to the force sensor. We detect the main frequency f_{1st} in all the tests. However, a second frequency appears at $f_{2nd} \approx 43.50$ Hz. Therefore, f_{1st} and f_{2nd} are the first and the second natural frequencies of the wing-base system depicted in Fig. 1.

As a simple theoretical model, one can estimate the natural frequency using as a model of the aluminum NACA0012 airfoil a flat plate with the same inertial thickness. The natural vibration frequencies for a rectangular aluminum plate were already obtained experimentally by [32]. The rectangular plate had an aspect ratio AR = 2, perfectly embedded in one of its short edges and free at the other. Dalley observed an eigenvalue of the vibration problem for the first natural mode $\lambda = \omega \cdot a2 \cdot \rho/D = 3.36$, where ω is the first mode frequency, a the length of the plate, ρ material density and $D = E \cdot h3/[12 \cdot (1 - \mu 2)]$ the bending modulus of the plate (E is the material Young modulus, h the plate thickness and μ the Poisson module). We consider an equivalent rectangular solid plate with the same moment of inertia I, the same cross-sectional area at and the same aspect ratio AR of our model, the NACA0012 airfoil. The equivalent plate shows an analytical free vibration frequency of 29.43 Hz for the first mode, very close to that obtained experimentally in our model. In addition, the frequencies of the first three natural vibration modes of the equivalent plate have been also calculated analytically by means of the formulation developed by [33]. For the equivalent rectangular solid aluminum plate described above, the frequency for the first symmetric deformation mode is 30.81 Hz. This first mode has the smallest characteristic frequency and it requires less energy input to be produced than other modes. The frequencies obtained for the second and the third natural vibration modes are 154.56 and 192.97 Hz, respectively. The theoretical values of frequency for the first deformation mode of the equivalent plate are again in agreement with experimental data obtained for the first natural frequency of the wing-base system, f_{1st}. The small differences between theoretical and experimental data may be primarily due to the difference among real and theoretical boundary conditions; and secondly, the difference between NACA0012 profile and its equivalent rectangular plate.

Figure 4 sums up all the experimental results. It shows the ratio between the PSD and the mean PSD for any value of Re_c and AoA. PSD stems from the temporal evolution of the net force measurements. We only depict normalized

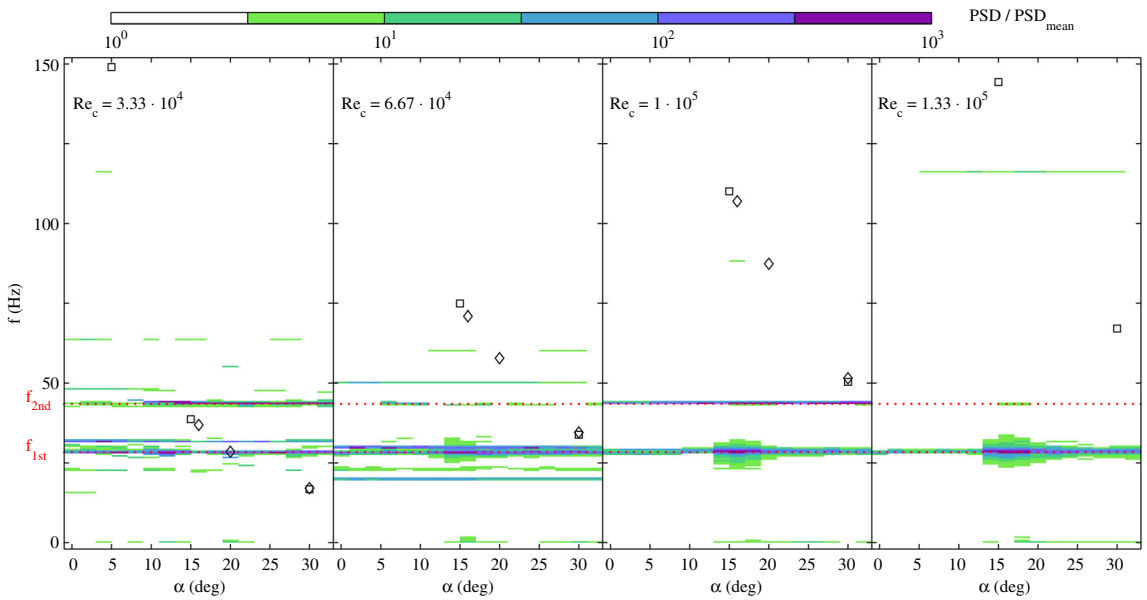

Fig. 4 Frequencies given by the normalized PSD (PSD/PSDmean) for four values of Re_c and several AoA from 0° to 35° together with the vortex shedding frequencies in the wake adapted from (12) and (17), plotted in squares and diamonds, respectively

PSD with power greater than five times the mean PSD. Moreover, we plot frequencies for vortex shedding in the near field of the wake reported by [8] and [9] in squares and diamonds, respectively. These data have been adapted from their Strouhal number data ($\mathrm{St} = f \cdot d/U_\infty$), where d is the length of the wing-section projection on the cross-stream direction. These authors observed that frequencies diminished as the AoA increased. However, the vibration of our model has a strong influence due to mechanical characteristics of the cantilever wing. The net aerodynamic force signal has two important sinusoidal components that correspond to natural frequencies of the wing-base in all cases ($f_{1st} \approx 28.25$ Hz and $f_{2st} \approx 43.50$ Hz). The presence of the most energetic peak at the first natural frequency is independent of the fluid flow around the model, while the peak at the second natural frequency is less dominant and its relative importance depends on Re_c and the AoA. Furthermore, our results could be compared with other work in which the dynamic response of a wing on-two-supports is dominated by the vortex shedding frequency [14]. They reported power peaks in the measured force signal at low frequencies ($f \approx 5$–10 Hz) regarding large-scale vortex formation (perpendicular to wingtip vortex) and emission in the wake at large AoA ($\alpha \geq 30°$ and $Re_c = 1.05 \times 10^4$). Unfortunately, our model offers PSD with peaks at natural frequencies f_{1st} and f_{2nd}. A possible explanation of this discrepancy could be the effect of the different type of airfoil support-setup base system of their experimental arrangement. Their research focused only on the dynamics of a wing on-two-supports, while our experimental study is based on mechanical vibrations produced by fluid structure interaction in a cantilever wing. Given the rigidity of our model, it is evident the strong influence of the mechanical behavior. Nevertheless, we could find very low and high frequencies which will be analyzed in detail below. We first focus on the effects caused by Reynolds number and AoA.

We depict in Fig. 5 the power spectral density (PSD) as function of frequency for two Reynolds numbers: $Re_c = 3.33 \times 10^4$ (a) and $Re_c = 1.33 \times 10^5$ (b), and for several AoA between 0° and 30°. For the lowest Re_c case, the power level of the signal does not depend on the AoA and remains almost constant. For the highest Reynolds number, one can observe again that the PSD remains almost constant at AoA lower than $\alpha = 14°$. Once the (stall) critical point is achieved, the power spectrum is one order of magnitude greater than those presented at low AoA, being more significant at low frequencies. For AoA beyond 20°, the power decreases again, although it continues being more energetic than those given for pre-stall angles. In any case, note that peaks obtained from natural frequencies do not depend on AoA or Re_c.

The increment in the PSD shown in Fig. 5 caused by the vibration process at stall angles is a consequence of the change in the overall 2D flow characteristics, specially on the flow regime in the suction surface of the NACA 0012 airfoil, and the subsequent emission of shear layer instabilities. Laminar separation regime (without subsequent reattachment) dominate the flow at AoA lower than 3°–5° for any value of Re_c considered in this work (see also [12]). As the AoA increases beyond a certain threshold, the separated boundary layer reattaches to the surface, thus forming the characteristic LSB on the surface. At these flow regimes, the fundamen-

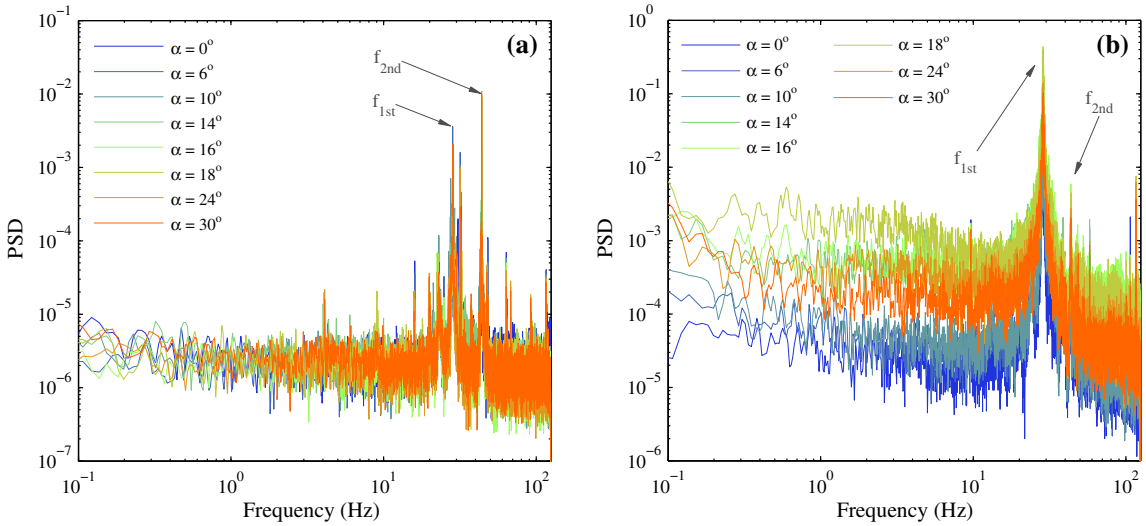

Fig. 5 PSD for $Re_c = 3.33 \times 10^4$ (**a**) and $Re_c = 1.33 \times 10^5$ (**b**) for AoA between 0° and 30°

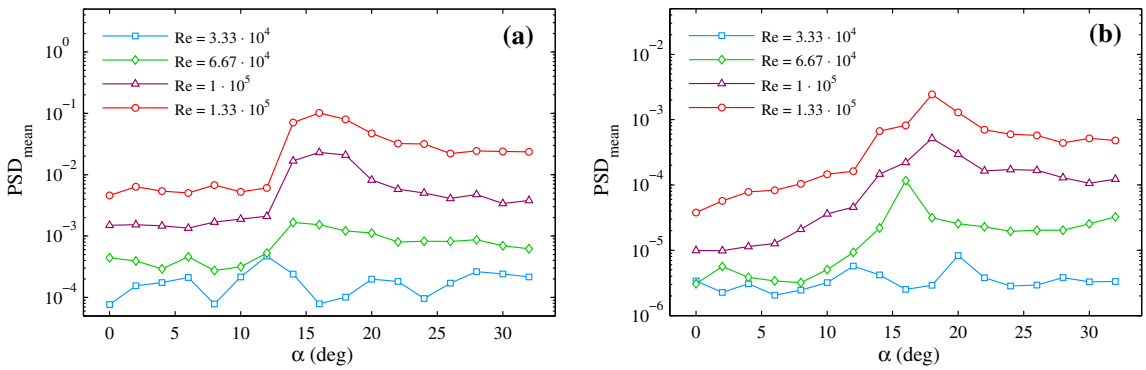

Fig. 6 Mean PSD for the first mechanical frequency $f_{1st} = 28.25 \pm 1.00$ Hz (**a**) and for the lowest frequencies interval flow = [0.005, 2.000] Hz (**b**)

tal frequency of shear-layer disturbances depends strongly on the Re_c and weakly on the AoA, but it does not show sudden variations [8, 34, 35]. However, the separation bubble burst and the resulting transition from LSB regime to a turbulent separated boundary layer, which occurs at the stall angle, causes a sharp drop on the fundamental frequency of the shear layer instabilities [36, 37]. This sudden perturbation on the flow characteristics excite the first natural frequency f_{1st} of the cantilever wing (see Fig. 4) since this frequency need the lowest amount of energy to gain power, leading to an increment in the wing vibration amplitude. Thus, the PSD level increases for the whole force signal at the turbulent separation regime (AoA slightly greater than the stall point). The absence of power increment for the lowest Reynolds number together with the lack of a marked drop on the lift coefficient at the stall angle, suggests that turbulent reattachment near the separated shear layer does not fully occur at the NACA 0012 suction surface since this case is slightly lower than the critical Reynolds number for the LSB formation [8, 38]. To provide a better understanding of these points, Fig. 6a shows the mean PSD of the net force for the first mechanical frequency $f_{1st} = 28.25 \pm 1.00$ Hz, whilst Fig. 6b depicts the mean PSD for the lowest frequencies interval flow = [0.005, 2.000] Hz. There is a increment of power as Re_c increases, but this may be explained due to an increase of the turbulent kinetic energy transported by increasing the value of the free-stream velocity. However, the PSD for the first natural frequency presents a sudden increment when approaching stall, followed by a slow decrease with the AoA, especially for Re_c greater than 1×10^5. This change in the power produces the first natural vibration mode of the cantilever wing to become significant in the dynamic response at stall angles as shown in Fig. 4. Consequently, force fluctuations increment their values as also shown in

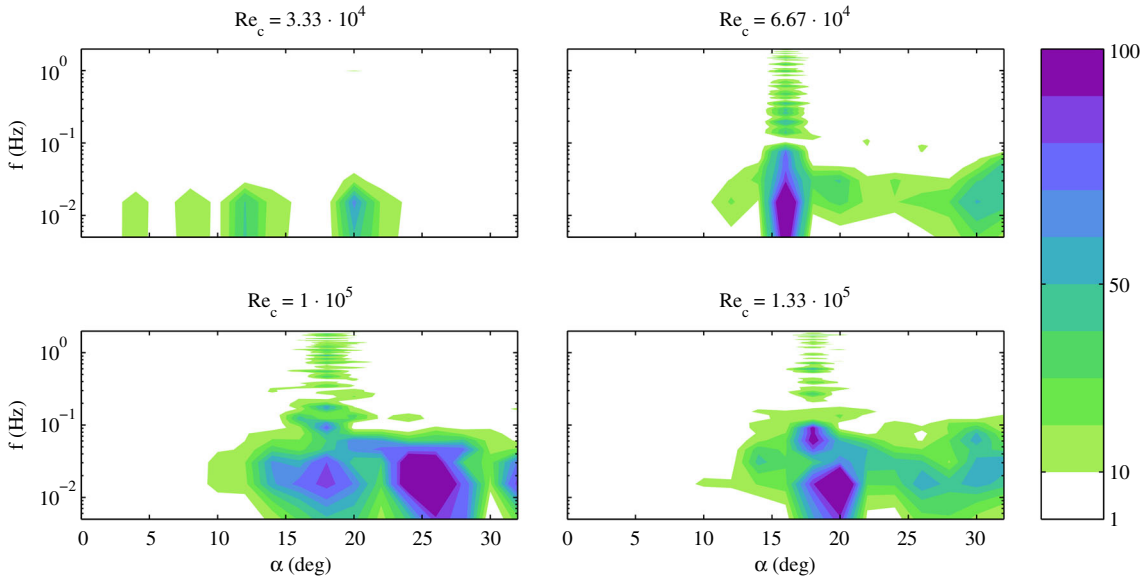

Fig. 7 Normalized PSD for any value of Re_c at very low frequencies in the range between 0.005 and 2 Hz

Fig. 2. The reader must notice that this critical Reynolds number $Re_c = 1 \times 10^5$ is also connected to the aerodynamic characteristics [28], at which β_{L1} saturates its value and the polar curve changed its trend, the parameter β_{L1} being the linear slope between C_L and α for AoA lower than 3°, (see, [28]). Finally, note that comparing Fig. 6a, b we observe that the maximum PSD is reached as AoA increases for frequencies between 0.005 and 2.000 Hz (b) in a smoother form than that obtained from the first natural frequency, f_{1st} (a). This feature stems from the fact that the presence of the stall angle not only strongly affects the power increment at these low frequencies, but also other flow phenomena could be relevant. This analysis will be carried out in the following section.

3.1 Dynamic Response at Very Low Frequencies

In order to characterize with detail the energy presented at very low frequencies, a new signal is developed by a low-pass 2 Hz filter. Thus, the components of longer time periods are isolated for each AoA and Reynolds number. To improve the experimental observations given in Fig. 4, Fig. 7 shows the PSD of the filtered net force signal ($f \leq 2$ Hz) normalized by the mean power in a logarithmic scale. Peaks appear for frequencies lower than 0.2 Hz, and for any value of the Reynolds number, particularly at large AoA. This low frequency corresponds to the typical development of the wingtip vortex as the AoA increases for $Re_c = O(10^5)$ (see [4]). The value of the most energetic frequency is also in agreement with the experimental results reported in a previous paper [39]. In their work, there was a vortex centroid position variation (called vortex meandering) at the plane perpendicular to the flow direction, its frequency being lower than 0.2 Hz for axial positions, x/c, ranging from 0 to 4 (near field) and $22504 \leq Re_c \leq 41874$. For the same phenomenon and using PIV measurements, [40] also reported values for the fundamental frequency of the vortex center variation slightly lower than 1 Hz in a plane located at $x/c = 11.2$ (far field) from a wing model of AR = 5 and $Re_c \sim O(106)$. Therefore, the observed low-frequency peaks on the forces exerted over the wing are also connected to this spatial fluctuation of the wingtip vortex behind the NACA0012 airfoil. The authors do believe that the exact value of 1 or 0.2 Hz is not the key point because this low frequency strongly depends on the Reynolds number considered and also the aspect ratio. For this reason, we claim for the order of magnitude of this low frequency but not for the exact value. In fact, [11] reported numerical frequencies equal to 0.13 and 0.62 Hz for AoA = 9.25° and 12°, respectively, for a 2D NACA 0012 profile at $Re_c = 5 \times 10^4$. These values prove again that this complex problem in the dynamic response may be characterized taking into account the order of magnitude of these low frequencies.

3.2 Dynamic Response at High Frequencies

Though the first two natural frequencies, f_{1st} and f_{2nd}, are significant and they dominate the whole dynamic response at $Re_c = 1 \times 10^5$ in our rigid model as shown in Fig. 4, several energetic and secondary frequencies are present for the two lowest Reynolds numbers near the first two natural frequencies but much less energetic than the natural ones. For this reason, we pay our attention on the interval of high frequencies, from 45 to 125 Hz. As we commented above for

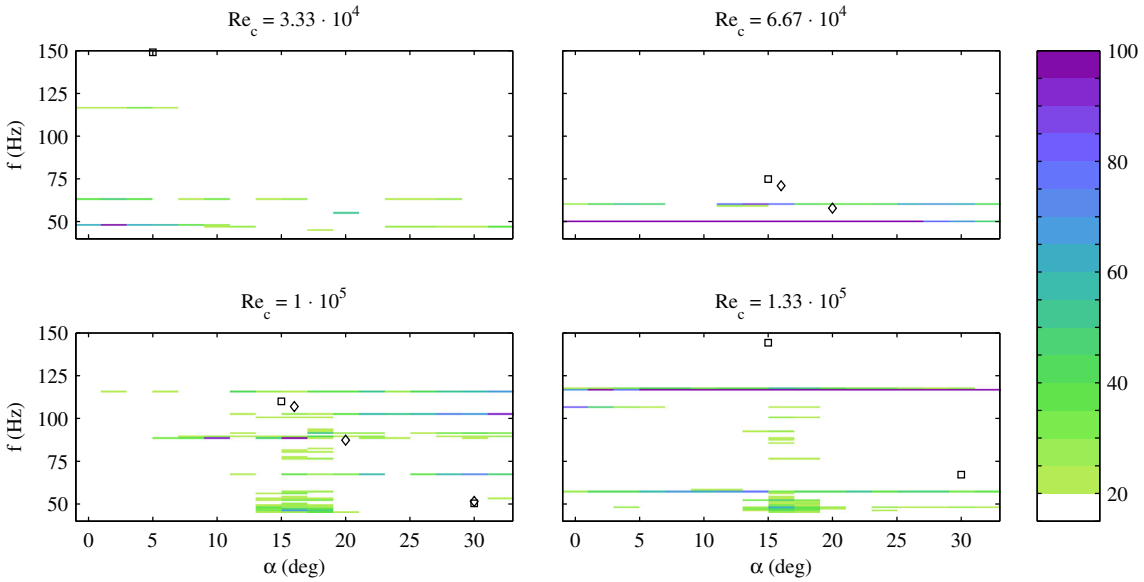

Fig. 8 Normalized PSD for any value of Re_c at high frequencies in the range between 45 and 125 Hz

the low-frequency analysis, we filter again the PSD signal in the range of high frequencies for all the Reynolds numbers and AoA. The results are depicted in Fig. 8 together with those vortex shedding results given by [8] and [9] from Fig. 4. It is observed a reasonably good agreement between our results and those frequencies reported by these authors. As Re_c increases, and consequently vortex shedding frequencies, these secondary components in the force signal around f_{1st} and f_{2nd} smoothly increase their influence. For the highest Reynolds number, the power peak at f_{2nd} disappears, and a new frequency becomes important at $\sim$116.25 Hz. The reader must note that the values of high frequency peaks obtained from the PSD plot increases with Reynolds number and always for AoA greater to the stall angle. Our observations also give us values of predominant frequencies close to the natural modes.

Furthermore, [38] detected Tollmien-Schlichting waves for $Re_c \leq 1 \times 10^5$ in the laminar-to-turbulent transition in the boundary layer with a main frequency of 32 Hz in the vicinity of the leading edge for a NACA 0012 airfoil and small AoA. Regarding our results, a power peak near to this frequency is also detected for the two lowest Re_c, primarily at small angles of attack (see again Fig. 4). Moreover, and according to their results, the shear layer instability wave increased its frequency with the Reynolds number up to 53 and 88 Hz over the trailing edge. In our case, these unstable waves in the laminar shear layer may also explain the secondary frequencies observed beyond the natural ones in Fig. 8.

To sum up, our observations show that low frequencies depends on Reynolds number because they are different as Re increases. There is a gradual change in the peaks from $Re_c = 3.33 \times 10^4$ at which the Normalized PSD do not show high values to Re_c greater than 6.67×10^4. In this range of high Re_c the peaks are less scattered for AoA greater than the stall angle.

4 Conclusions

The precise dynamic response of low-aspect-ratio NACA0012 wing model at low Reynolds numbers has been characterized by a digital force sensor. We compute C_D, C_L and the PSD signal using the temporal evolution of the force measurements.

The aerodynamic characteristics show that there is a sudden increase in the standard deviation obtained from the lift coefficient σL that appears from $\alpha_{stall} \leq \alpha \leq \alpha^*$, being $\alpha_{stall} = 12^o$ the stall angle and α^*, between 16º and 18º, depending on Re_c. We observe that α^* decreases slightly with Re_c. We claim that this sudden increase is related to a two-dimensional effect that corresponds to the formation of a turbulent boundary layer in the suction wall, as reported numerically in the State of Art. Afterwards, the fluctuations in the lift force decrease with α up to 22º. A plausible explanation is the 2D effect of pulsating LSB and subsequent downstream propagation of LEV. The same behavior in the standard deviation has been observed for the drag coefficient, C_D, except for the lowest Re_c studied because the turbulent flow does not attain for the LSB on the suction wall.

The wing dynamic response shows two natural frequencies f_{1st} and f_{2nd} of 28.25 Hz and 43.50 Hz, respectively, which are found regardless the values of the AoA and Re_c. They correspond to the natural frequencies of the wing-base system model. This result seems to be evident since our

model is rigid. On the other hand, the mean PSD level experiences a sudden increase with Re_c for AoA belonging again to the range αstall $\alpha_{stall} \leq \alpha \leq \alpha^*$, particularly for Reynolds numbers greater than 1×10^5. However, the PSD level does not depend on the AoA for the lowest Reynolds number considered because there is no unstable LSB at the suction wall for $Re_c = 3.3 \times 10^4$. Finally, spectral density local peaks are found for frequencies lower than 0.2 Hz for any value of Re_c. These low-level frequencies appear approaching stall and they can be observed on the wingtip phenomenon that produces a random movement of the vortex core behind the wing. Finally, high frequencies close to $O(10^2)$ Hz are linked to the formation and emission of coherent turbulent structures in the near field of the wake since they are in agreement with other authors' results. Thus, only 2D effects explain the formation of these high frequencies.

Acknowledgement This research has been supported by Proyecto de Excelencia de la Junta de Andaluc´ıa, Grant number P11-TEP-7776. Authors thank Luc´ıa Luque for her corrections in the English style.

References

1. Mueller TJ (1999) Aerodynamics measurement at low Reynolds numbers for fixed wing micro-air vehicles. In: Materials on the RTO AVT special course on development and operation of UAVs for military and civil applications. pp 1–32, VKI, Belgium, Sept 13–17
2. Mueller TJ, Torres GE (2001) Aerodynamics of low aspect ratio wings at low Reynolds numbers with application to micro-air vehicles design an optimization. In: Final Report UNDAS-FR-2025. pp 1–126, Naval Research Laboratory, Washington D.C., USA
3. Lee T, Su YY (2012) Wing tip vortex control via the use of a reverse half-delta wing. Exp Fluids 52:1593–1609
4. Lee T, Pereira J (2013) Modification of static-wing tip vortex via a slender half-delta wing. J Fluids Struct 43:1–14
5. Gad-el Hak M (1990) Control of low-speed airfoil aerodynamics. AIAA J 28(9):1537–1552
6. Mueller TJ (1985) Low Reynolds number vehicles. In: Report AGARD-AG-288. p 69, Advisory Group for Aerospace Research and Development, North Atlantic Treaty Organization, France
7. Huang RF, Lee HW (1999) Effects of freestream turbulence on wing-surface flow and aerodynamic performance. J Aircr 36(9):965–972
8. Huang RF, Lin C (1995) Vortex shedding and shear-layer instability of wing at low-Reynolds numbers. AIAA J 33(8):1398–1403
9. Lee HW, Huang RF (1998) Frequency selection of wake flow behing a NACA 0012 wing. J Mar Sci Technol 6(1):29–37
10. Huang RF, Lee HW (2000) Turbulence effects on frequency characteristics of unsteady motions in wake of wing. AIAA J 38(1):85–93
11. Rodríguez I, Lehmkuhl O, Borrell R, Oliva A (2013) Direct numerical simulation of a NACA0012 in full stall. Int J Heat Fluid Flow 43:194–203
12. Yen SC, Huang LC (2009) Flow patterns and aerodynamics performance of unswept and swept-back wings. J Fluids Eng 131(11):111101-1–111101-10
13. Sharma A, Visbal M (2017) Numerical investigation of the effect of airfoil thickness on onset of Dynamic stall. Cornell University Library, Ithaca, pp 1–32
14. Mahbub Alam M, Zhou Y, Yang HX, Guo H, Mi J (2010) The ultra-low Reynolds number airfoil wake. Exp Fluids 48:81–103
15. Zhou Y, Mahbub Alam M, Yang HX, Guo H, Wood DH (2011) Fluid forces on a very low Reynolds number airfoil and their prediction. Int J Heat Fluid Flow 32:329–339
16. Poirel D, Harris Y, Benaissa A (2008) Self-sustained aeroelastic oscillations of a NACA 0012 airfoil at low-to-moderate Reynolds numbers. J Fluids Struct 24:700–719
17. Kim DH, Chang JW (2014) Low-Reynolds-number effect on the aerodynamic characteristics of a pitching NACA 0012 airfoil. Aerosp Sci Technol 32(1):162–168
18. Poirel D, Yuan W (2010) Aerodynamics of laminar separation flutter at a transitional Reynolds number. J Fluids Struct 26:1174–1194
19. Rojratsirikul P, Wang Z, Gursul I (2010) Effect of pre-strain and excess length on unsteady fluid structure interactions of membrane airfoils. J Fluids Struct 26:359–376
20. Rojratsirikul P, Genc MS, Wang Z, Gursul I (2011) Flow-induced vibrations of low aspect ratio rectangular membrane wings. J Fluids Struct 27:1296–1309
21. Moreau DJ, Brooks LA, Doolan CJ (2012) The effect of boundary layer type on trailing edge noise from sharp-edged at plates at low-to-moderate Reynolds number. J Sound Vib 331:3976–3988
22. PeiChong T, Joseph PF (2013) An experimental study of airfoil instability tonal noise with trailing edge serrations. J Sound Vib 332:6335–6358
23. Moreau DJ, Prime Z, Porteous R, Doolan CJ, Valeau V (2014) Flow-induced noise of a wall-mounted finite airfoil at low-to-moderate Reynolds number. J Sound Vib 333:6924–6941
24. Devenport WJ, Staubs JK, Glegg SAL (2010) Sound radiation from real airfoils in turbulence. J Sound Vib 329:3470–3483
25. Ikeda T, Atobe T, Takagi S (2012) Direct simulations of trailing-edge noise generation from two-dimensional airfoils at low Reynolds numbers. J Sound Vib 331:556–574
26. Bertagnolio F, Fischer A, Zhu W (2014) Tuning of turbulent boundary layer anisotropy for improved surface pressure and trailing-edge noise modeling. J Sound Vib 333:991–1010
27. Fedoul F, Parras L, del Pino C, Fernandez-Feria R (2014) Experimental study of the aerodynamic characteristics of a low-aspect-ratio at plate array in a configuration of interest for a tidal energy converter. J Fluids Struct 48:487–496
28. Martinez-Aranda S, Garcia-Gonzalez A, Parras L, Velazquez-Navarro J, del Pino C (2016) Comparison of the aerodynamic characteristics of the NACA 0012 airfoil at low-to-moderate Reynolds numbers for any aspect ratio. Int J Aerosp Sci 4(1):1–8
29. Kline SJ, McClintock FA (1953) Describing uncertainties in single-sample experiments. Mech Eng 75(1):3–8
30. Goldstein RJ (1983) Fluid Mechanics Measurements. Hemisphere Publishing Corporation, USA
31. Ngo HT, Barlow LE (2002) Lifting surface with active variable tip member and method for influencing lifting surface behavior therewith. In: United State Patent No. US 6.394.397 B1. pp 1–10, May 28
32. Dalley IW, Ripperger EA (1952) Experimental values of natural frequencies for skew and rectangular cantilever plates. ProcSoc Exp Stress Anal 9(2):51–66
33. Warburton GB (1954) The vibration of rectangular plates. Proc Inst Mech Eng 168(12):371–384
34. Yarusevych S, Sullivan PE, Kawalls JG (2009) On vortex shedding from an airfoil in low-Reynolds-number flows. J Fluid Mech 632:245–271
35. Yarusevych S, Boutilier MSH (2011) Vortex shedding of an airfoil at low Reynolds-numbers. AIAA J 49(10):2221–2227
36. Boutilier MSH, Yarusevych S (2013) Parametric study of separation and transition characteristics over an airfoil at low Reynolds numbers. Exp Fluids 52(6):1491–1506

37. Gerakopulos RJ (2011) Investigating flow over an airfoil at low Reynolds numbers using novel time-resolved surface pressure measurements. In: PhD. Doctoral Tesis. University of Waterloo, Ontario, pp 1–152
38. Kim D-H, Yang J, Chang J-W, Chung J (2009) Boundary layer and near-wake measurements of NACA 0012 airfoil at low Reynolds numbers. In: 47th AIAA Aerospace Sciences Meeting. pp 1–12, Orlando, Florida USA
39. del Pino C, Lopez-Alonso JM, Parras L, Fernández-Feria R (2011) Dynamics of the wing-tip cortex in the near field of a NACA 0012 airfoil. Aeronaut J 115(1166):229–239
40. Roy C, Leweke T (2008) Experiments on vortex meandering. In: International Workshop on Fundamental Issues Related to Aircraft Wakes, Marseille, France, May 27–29